Enclathration by a xanthenol host *via* solid–solid reactions: structures and kinetics†

Ayesha Jacobs,*[a] Luigi R. Nassimbeni,[a] Kanyisa L. Nohako,[a] Gaelle Ramon[a] and Jana H. Taljaard[b]

Received (in Montpellier, France) 2nd April 2009, Accepted 18th June 2009
First published as an Advance Article on the web 14th July 2009
DOI: 10.1039/b906720e

The host compound 9-(4-methoxyphenyl)-9*H*-xanthen-9-ol (H) forms inclusion compounds with the solid guests 1-naphthylamine, 8-hydroxyquinoline, triethylenediamine and acridine. All four structures were successfully solved in the triclinic spacegroup $P\bar{1}$. Similar packing motifs arise for the 1-naphthylamine and the 8-hydroxyquinoline inclusion compounds where the main interaction is of the form (host)–OH···O–(host). Both the triethylenediamine and the acridine guests hydrogen bond to the host molecule. The thermal stabilities and kinetics of the solid–solid reactions were determined.

Introduction

Solid–solid reactions, or reactions carried out in the absence of solvent, are interesting because they are environmentally benign. Significant early work in this field was carried out by Rastogi and co-workers,[1,2] who studied a variety of reactions between organic reactants and summarised the kinetic equations and the factors affecting the reactivity of various systems. Toda and co-workers carried out a large number of such reactions and reported the formation of organic host–guest complexes,[3] Baeyer–Villiger oxidation of ketones,[4] Grignard reactions[5] and charge-transfer complexes.[6] Jones *et al.*[7] introduced the "solvent drop" method in these reactions and demonstrated the improvement in the rate of product formation. The mechanism of such reactions is not completely understood, and Scott *et al.* have pointed out the importance of the formation of a liquid phase when solids are ground together.[8,9] The solvent-free method has been employed to form supramolecular nano-capsules,[10] and a wide array of metal complexes, coordination clusters, and metal–organic frameworks[11]. Recently James and Pichon outlined an array-based system for the study of reacting solids.[12]

In this work we present the structures and kinetics of the inclusion compounds formed between the host H = 9-(4-methoxyphenyl)-9*H*-xanthen-9-ol and the solid guests 1-naphthylamine (NAPA), 8-hydroxyquinoline (HQ), triethylenediamine (TEDA) and acridine (ACR). The host atomic numbering and the guests are shown in Chart 1.

[a] *Department of Chemistry, Cape Peninsula University of Technology, PO Box 652, Cape Town, South Africa. E-mail: jacobsa@cput.ac.za; Fax: +27 21 460 3854; Tel: +27 21 460 3167*
[b] *Sasol Technology, R&D, Klasie Havenga Road 1, Sasolburg, South Africa*

† CCDC reference numbers 736889–736892. For crystallographic data in CIF or other electronic format see DOI: 10.1039/b906720e

Results and discussion

Structures

The single crystal structures of the inclusion complexes formed between H and each guest were examined and the crystal and refinement data are presented in Table 1. The structure of H·½NAPA crystallises in the space group $P\bar{1}$ with one host molecule in general positions and the 1-naphthylamine guest located on a centre of symmetry at Wyckoff position *g*. The guest is disordered but was successfully modelled by imposing a series of bond-length constraints while the non-hydrogen atoms were allowed to refine isotropically. However we note that there was residual electron density which our model did not take into account.

A similar situation is obtained for the structure of the 8-hydroxyquinoline compound H·½HQ. In this case the disordered guest is located on a centre of inversion which is coincident with the midpoint common to the two rings. The hydroxyl moieties and the nitrogen atom are therefore disordered over two positions with equal site occupancies. The packing of the structure H·½HQ is shown in Fig. 1.

The host molecules form centrosymmetric dimers *via* O2–H1···O1 hydrogen bonds. Details of the hydrogen bonding metrics are given for this and other structures in Table 2. Both the 1-naphthylamine and the 8-hydroxyquinoline guests occupy channels parallel to [010].

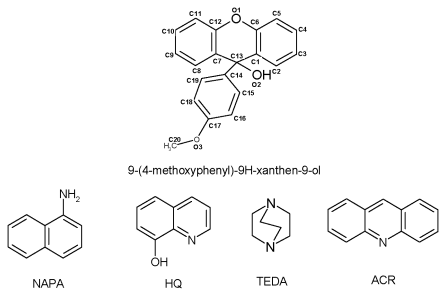

Chart 1 Host atomic numbering and guests.

Table 1 Crystal data table

	H·½NAPA	H·½HQ	H·½TEDA	H·ACR
Compound	H[a]·½$C_{10}H_9N$	H[a]·½C_9H_7NO	H[a]·½$C_6H_{12}N_2$	H[a]·$C_{13}H_9N$
M/g mol^{-1}	375.42	376.90	360.42	483.54
T/K	173	173	173	173
Crystal system	Triclinic	Triclinic	Triclinic	Triclinic
Space group	$P\bar{1}$	$P\bar{1}$	$P\bar{1}$	$P\bar{1}$
a/Å	8.4231(17)	8.3982(17)	9.057(18)	10.607(2)
b/Å	9.0634(18)	8.9905(18)	9.6751(19)	11.247(2)
c/Å	13.014(3)	12.954(3)	10.501(2)	11.967(2)
α/°	96.60(3)	96.36(3)	88.56(3)	96.17(3)
β/°	91.87(3)	91.64(3)	83.74(3)	110.43(3)
γ/°	109.87(3)	109.14(3)	85.45(3)	111.08(3)
V/Å^3	925.4(3)	916.1(3)	911.7(3)	1203.2(4)
Z	2	2	2	2
μ/mm^{-1}	0.088	0.092	0.086	0.085
F(000)	395	395	382	508
Reflections collected/unique	15 208/3505	13 605/3435	15 587/3431	20 116/4553
ρ_{calc}/g cm^{-3}	1.347	1.366	1.313	1.335
Final R indices	R_1 = 0.1109,	R_1 = 0.0551,	R_1 = 0.0379,	R_1 = 0.0420,
[$I > 2\sigma(I)$]	wR_2 = 0.3526	wR_2 = 0.1349	wR_2 = 0.0914	wR_2 = 0.0964
R indices (all	R_1 = 0.1471,	R_1 = 0.0796,	R_1 = 0.0538,	R_1 = 0.0660,
data)	wR_2 = 0.3939	wR_2 = 0.1544	wR_2 = 0.1003	wR_2 = 0.1108
Largest difference peak and hole /e Å^{-3}	1.466 and −0.730	0.971 and −0.465	0.192 and −0.210	0.168 and −0.222

[a] $C_{20}H_{16}O_3$.

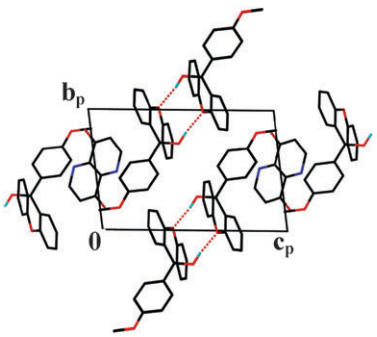

Fig. 1 Packing diagram of H·½HQ down [100]. Hydrogens have been omitted for clarity.

Although the stoichiometry of the H·½TEDA compound is the same as that of the two previous compounds the packing is substantially different, in that this structure displays host–guest hydrogen bonding (Fig. 2). The TEDA guest lies in cavities on a centre of inversion at Wyckoff position *h*, and the ethylenic carbons are all disordered over two positions.

The structure with the acridine guest has a different stoichiometry with a host : guest ratio of 1 : 1. There is a (host)–OH···N(guest) hydrogen bond as shown in Fig. 3. The acridine is not disordered and occupies channels parallel to [100] and [001].

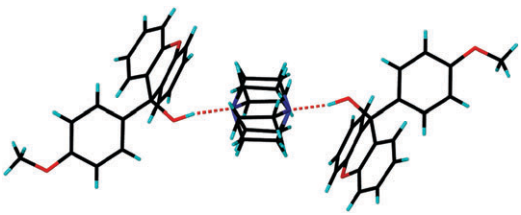

Fig. 2 Hydrogen bonding in H·½TEDA.

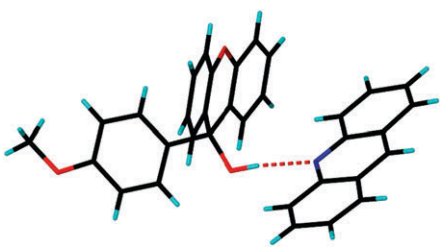

Fig. 3 Hydrogen bonding in H·ACR.

We have employed the program Crystal Explorer which calculates the Hirschfeld surfaces of a molecule in a crystal structure and depicts all the molecular interactions of a given targeted molecule with its neighbours.[13–16] In this work we have chosen the host molecule as the target in each of the four structures and the ensuing fingerprint plots are shown in

Table 2 Hydrogen bond data

	D–H···A	D–H/Å	H···A/Å	D···A/Å	D–H···A/°
H·½NAPA	O2–H1···O1[a]	0.96(4)	1.91(4)	2.864(4)	171(3)
H·½HQ	O2–H1···O1[b]	0.96(2)	1.92(2)	2.863(2)	168(2)
H·½TEDA	O2–H1···N1G	0.94(2)	1.86(2)	2.784(2)	169(2)
H·ACR	O2–H1···N1G	0.90(2)	2.08(2)	2.966(2)	170(2)

[a] −x, −y, −z + 2. [b] −x, −y, −z + 1.

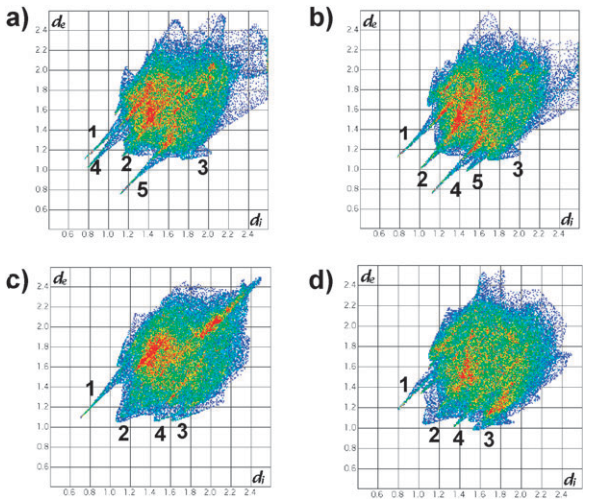

Fig. 4 Fingerprint plots for the surfaces generated for the host molecules only (a) H·½NAPA, (b) H·½HQ, (c) H·½TEDA and (d) H·ACR.

Fig. 4(a–d). The peaks in the figures are associated with various host···guest and host···host interactions which are summarised in Table 3. Thus peak 1 corresponds to the hydrogen bond (host)OH···O(host) in H·½NAPA and H·½HQ, and to (host)OH···N(guest) in H·½TEDA and H·ACR. Peak 2 corresponds to H···H interactions while peak 3 is associated with C···H interactions. In Fig. 4a peak 4 arises from the interaction of a host hydrogen with a disordered carbon of the guest. Peak 5 is the hydrogen bond occurring between the targeted host and a neighbouring host molecule. In Fig. 4b peak 4 is the hydrogen bond discussed previously and peak 5 is associated with the interaction of the host methoxy oxygen with the hydroxyl hydrogen of the guest. In Fig. 4c and 4d the small peak 4 is due to the interaction of the host pyranyl oxygen with a neighbouring host hydrogen.

Thermal analysis

We analysed the thermal profiles of the single crystals, grown from solution, of each inclusion compound by differential scanning calorimetry (DSC). Each compound yielded a single endotherm corresponding to its melting point. These are reported in Table 4 together with the melting points of the apohost and each of the solid guests. We note that the melting points of the inclusion compounds are always higher than that of the host or the respective guest. In particular the H·½TEDA compound is significantly stable with the melting point 48 K higher than that of the apohost, and this may be attributed to the fact that the host–guest system is stabilised by two hydrogen bonds and the TEDA guest occupies cavities.

Table 3 Summary of host···host and host···guest interactions shown in Fig. 4

Peak	H·½NAPA		H·½HQ		H·½TEDA		H·ACR	
% Host···host/guest								
1	5.1	OH···O	7.2	OH···O	1.6	OH···N	2.4	OH···N
2	44.7	H···H	52.2	H···H	49.3	H···H	54.0	H···H
3	9.1	C···H	13.9	C···H	9.7	C···H	18.9	C···H
4	19.6	H···C	8.7	O···HO	5.7	O···H	7.0	O···H
5	5.9	O···HO	8.7	O···HO				

Kinetics of solid–solid reactions

The PXRD results for the H·½NAPA grinding experiments are shown in Fig. 5. The growth of a peak at $2\theta = 6.8°$ was monitored with time and the diamond calibrant shows a peak at $2\theta = 43.9°$. The results of the solid–solid reactions are shown in Fig. 6 in which we plotted $\ln(1-\alpha)$ *vs.* time, where α represents the extent of reaction as measured by the normalised intensity of a targeted diffraction peak of the product. This is a common method of analysis, as adopted by Lipkowski *et al.*, for the enclathration of xylene isomers by a Werner clathrate.[17] The rate constants for the solid–solid reactions, carried out at ambient temperature (25 °C) were:

H·½NAPA $k = 1.85 \times 10^{-2}$ min^{-1}
H·½HQ $k = 2.20 \times 10^{-2}$ min^{-1}
H·½TEDA $k = 2.51 \times 10^{-2}$ min^{-1}
H·ACR $k = 6.10 \times 10^{-3}$ min^{-1}

The kinetics for the H·ACR reaction are significantly slower than those of the other three compounds. We note that the vapour pressure of acridine at 25 °C is estimated to be significantly lower than that of the other three guests.[18]

Friščič and Jones have recently reviewed the mechanism of co-crystal formation *via* grinding.[19] They point out that molecular diffusion, eutectic formation and the formation of an amorphous phase may all be important. In the reaction of picric acid with aromatic hydrocarbons, Rastogi *et al.*[20] noted that surface migration and vapour diffusion were the principal mechanism. Kuroda and co-workers[21] also showed that this was the mechanism which operated in the reaction of *p*-benzoquinone with 2,2′-biphenol and its isomer 4,4′-biphenol. The kinetics of the solid–solid reaction between the host 1,1,6,6-tetraphenylhexa-2,4-diyne-1,6-diol with benzophenone were measured by infrared spectroscopy, and the reaction was achieved by shaking powdered samples of host and guest in a test tube. This reaction proceeds *via* vapour diffusion of the benzophenone, which has a relatively high vapour pressure of 8.2×10^{-4} torr at 25 °C.[22]

The structure of the apohost has been elucidated.[23] This compound crystallises in the space group $P2_1/c$ with $Z = 8$, with two independent molecules in the asymmetric unit. The structure comprises centrosymmetric hydrogen bonded dimers, with the hydroxyl moiety of one molecule hydrogen bonded to the pyranyl oxygen of a neighbouring molecule. In addition long chains of molecules are stabilised by a similar hydrogen bonded interaction. In the circumstances it is difficult to hypothesise on the mechanism of the solid–solid reactions which yield the host–guest products. We note however that the hydrogen bonded dimer motif is retained in both the H·½NAPA and H·½HQ structures. However in the H·½TEDA and the H·ACR compounds this is changed to a host–OH···N(guest) interaction.

Table 4 Thermal analysis data

Inclusion compound	H·½NAPA	H·½HQ	H·½TEDA	H·ACR
DSC (T_{on}/K)	413.4	399.2	443.0	426.9
Melting point of guest/K	322.2	346.5	429.7	380.7
Melting point of H/K	395.2	—	—	—

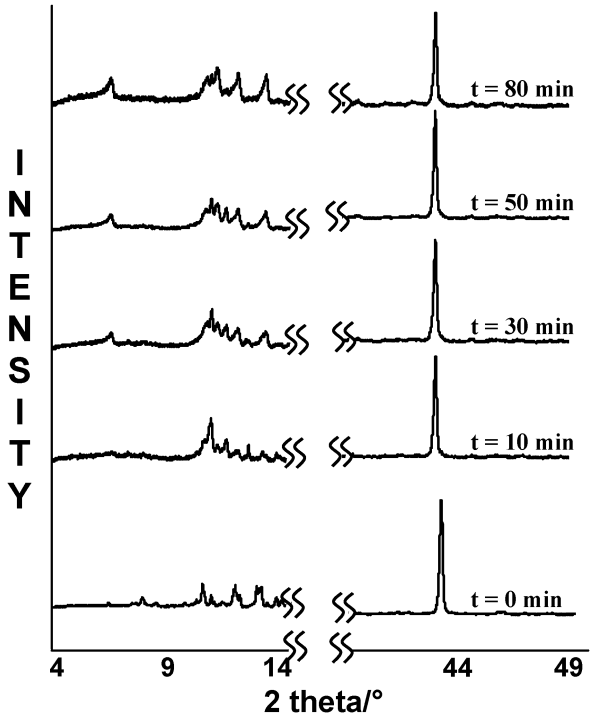

Fig. 5 PXRD plots for H·½NAPA.

Conclusions

The structures of the xanthenol host 9-(4-methoxyphenyl)-9*H*-xanthen-9-ol with the guests 1-naphthylamine (NAPA), 8-hydroxyquinoline (HQ), triethylenediamine (TEDA) and acridine (ACR) have been elucidated. They crystallise in two different packing motifs, with the H·½NAPA and H·½HQ exhibiting strong host–host H-bond interactions. The H·½TEDA and H·ACR structures, however, exhibit host–guest H-bonded interactions. The host–guest compounds were also formed by grinding of the two solids and the kinetics of the reactions were monitored by X-ray powder diffraction and followed the first order rate law $\ln(1 - \alpha) = -kt$ where α is the extent of reaction.

Experimental

Structure analysis

The host and each of the guest compounds were dissolved in ethanol and the saturated solutions were allowed to crystallise at room temperature. Cell dimensions were established from the intensity data measured on a Kappa CCD diffractometer using graphite-monochromated Mo-K_α radiation. The strategy for the data collections was evaluated using *COLLECT*[24] software. For all structures, the intensity data

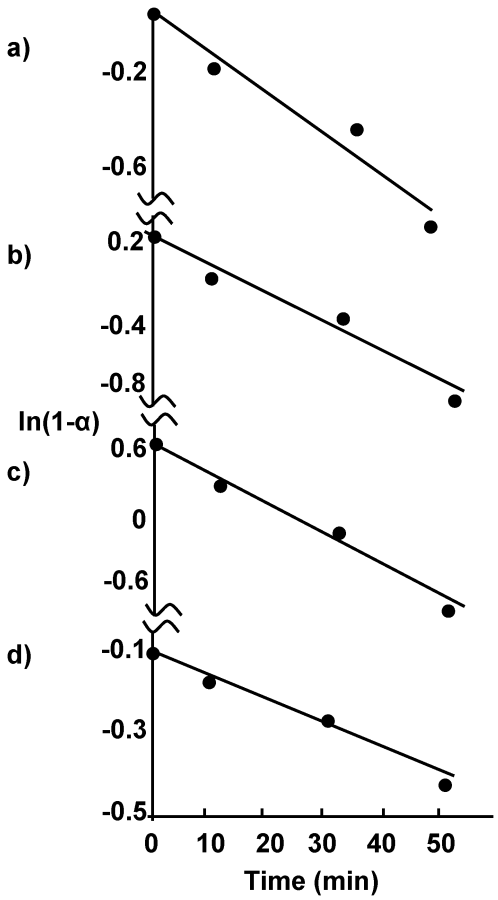

Fig. 6 First order kinetic plots for (a) H·½NAPA, (b) H·½HQ, (c) H·½TEDA and (d) H·ACR.

were collected by the standard phi scan and omega scan techniques and scaled and reduced using the program Denzo-SMN.[25] The structures were solved by direct methods and refined by full-matrix least-squares with SHELX-97[26] refining on F^2. The program X-Seed[27] was used as a graphical interface. Unless otherwise stated in the results and discussion section all the non-hydrogen atoms were refined anisotropically. The hydroxyl hydrogens were located in the difference electron density maps and refined with simple bond-length constraints[28] and the remaining hydrogen atoms were fixed in positions and refined isotropically.

Thermal analysis

Differential scanning calorimetry (DSC) was performed on a Perkin Elmer Pyris 6 system. The experiments were performed over the temperature range 303–573 K at a heating rate of 10 K min^{-1} with a purge of dry nitrogen flowing at

30 mL min^{-1}. The samples were crushed, blotted dry and placed in crimped but vented pans.

Grinding experiments

The grinding experiments were carried out with an agate mortar and pestle at room temperature. The starting quantities of the reactants were in the same stoichiometries as given by the crystal structure analyses. Samples were withdrawn at fixed periods of time and the ground powders analysed by PXRD on a Philips PW 1050/80 goniometer equipped with a PW3710 control unit using Cu K_α radiation.

We monitored the kinetics of the solid–solid reactions between the apohost and the various guests by selecting the appearance of a particular peak in the newly forming inclusion compound. We interrupted the grinding experiment at chosen intervals and added fixed quantities of diamond powder to the samples. This allowed us to measure the intensities of the targeted peak using the (111) peak of diamond as a calibrant.

Acknowledgements

We thank the NRF (Pretoria) and the Cape Peninsula University of Technology for funding.

Notes and references

1 R. P. Rastogi, *J. Sci. Ind. Res.*, 1970, **29**, 177.
2 R. P. Rastogi, N. B. Singh and R. P. Singh, *J. Solid State Chem.*, 1977, **20**, 191.
3 F. Toda, K. Tanaka and A. Sekikawa, *J. Chem. Soc., Chem. Commun.*, 1987, 279.
4 F. Toda, M. Yagi and K. Kiyoshige, *J. Chem. Soc., Chem. Commun.*, 1988, 958.
5 F. Toda, H. Takumi and H. Yamaguchi, *Chem. Express*, 1989, **4**, 507.
6 F. Toda and H. Miyamoto, *Chem. Lett.*, 1995, 861.
7 N. Shan, F. Toda and W. Jones, *Chem. Commun.*, 2002, 2372.
8 G. Rothenberg, A. P. Downie, C. L. Raston and J. L. Scott, *J. Am. Chem. Soc.*, 2001, **123**, 8701.
9 G. W. V. Cave, C. L. Raston and J. L. Scott, *Chem. Commun.*, 2001, 2159.
10 J. Antesberger, G. W. V. Cave, M. C. Ferrarelli, M. Heaven, C. L. Raston and J. L. Atwood, *Chem. Commun.*, 2005, 892.
11 A. L. Garay, A. Pichon and S. L. James, *Chem. Soc. Rev.*, 2007, **36**, 846.
12 A. Pichon and S. L. James, *CrystEngComm*, 2008, **10**, 1839–1847.
13 M. A. Spackman and J. J. McKinnon, *CrystEngComm*, 2002, **4**, 378.
14 J. J. McKinnon, M. A. Spackman and A. S. Mitchell, *Acta Crystallogr., Sect. B: Struct. Sci.*, 2004, **60**, 627.
15 J. J. McKinnon, D. Jayatilaka and M. A. Spackman, *Chem. Commun.*, 2007, 3814.
16 M. A. Spackman and D. Jayatilaka, *CrystEngComm*, 2009, **11**, 19–32.
17 J. Lipkowski, K. Suwinska, J. Hatt, A. Zielenkiewicz and W. Zielenkiewicz, *J. Inclusion Phenom.*, 1984, **2**, 317–325.
18 SciFinder Scholar (CAS) Advanced Chemistry Development Software V 8.14.
19 T. Friščič and W. Jones, *Cryst. Growth Des.*, 2009, **9**, 1621–1637.
20 R. P. Rastogi, P. S. Basci and L. S. Chandler, *J. Phys. Chem.*, 1963, **67**, 2569–2573.
21 R. Kuroda, K. Higashiguchi, S. Hasebe and Y. Imia, *CrystEngComm*, 2004, **6**, 463–468.
22 D. R. Bond, L. Johnson, L. R. Nassimbeni and F. Toda, *J. Solid State Chem.*, 1991, **92**, 68–79.
23 E. Curtis, L. R. Nassimbeni, H. Su and J. H. Taljaard, *Cryst. Growth Des.*, 2006, **6**, 2716–2719.
24 *COLLECT*, Data Collection Software; Nonius: Delft, The Netherlands, 1998.
25 Z. Otwinowski and W. Minor, *Methods in Enzymology, Macromolecular Crystallography, Part A*, ed. C.W. Carter and R.M. Sweet, Academic Press, New York, 1997, vol. 276, pp. 307–326.
26 G. M. Sheldrick, *SHELX97, Program for Crystal Structure Determination*, University of Göttingen, Germany, 1997.
27 L. J. Barbour, X-Seed, Graphical Interface for the SHELX program, *J. Supramol. Chem.*, 2003, **1**, 189.
28 I. Olovsson and P. Jönson, in *The Hydrogen Bond—Structure and Spectroscopy*, ed. P. Schuster, G. Zundel, C. Sardify, North Holland Publishing Company, Amsterdam, 1975.

